Biophysical Journal, Volume *111*

Supplemental Information

Macromolecular Crowding Modulates Actomyosin Kinetics

Jinghua Ge, Sherry D. Bouriyaphone, Tamara A. Serebrennikova, Andrei V. Astashkin, and Yuri E. Nesmelov

Supporting Information

Macromolecular crowding modulates actomyosin kinetics

J. Ge, S. D. Bouriyaphone, T. A. Serebrennikova, A. V. Astashkin, Y. E. Nesmelov

Ficoll70 slows actomyosin rigor binding. Effect of increased ionic strength of the solution.

To measure the rate of the rigor binding, we have rapidly mixed pyrene actin (0.5 μM) with myosin (various concentrations) and monitored the decrease in pyrene fluorescence associated with the rigor actomyosin complex formation [1]. The observed transients were fitted with single-exponential functions (Figure S1D). Similar to [2, 3], at a longer time scale, the transients were best fitted with a sum of an exponential and another function (polynomial or slow exponential with the rate independent of myosin concentration). The dependence of the reaction rate on the myosin concentration was fitted by a straight line, and the second order rate of actomyosin rigor binding was determined from the slope (Figure S2). The rate constant obtained without Ficoll70, $k_{+6}^{-F} = 1.68 \pm 0.05$ $\mu M^{-1}s^{-1}$, is in excellent agreement with the previous results for *D. discoideum* myosin [4-6]. With Ficoll70, the rate decreases seven-fold to 0.23 ± 0.03 $\mu M^{-1}s^{-1}$.

Ficoll70 increases the effective concentration of solutes and therefore affects the ionic strength of the solution. Actomyosin interaction depends on the ionic strength [7], and the decreased rate of the actomyosin interaction may reflect the increased ionic strength of the solution. Assuming the activity coefficient $\gamma = 2.5$ [8], the ionic strength of our buffered solution changes from 59 mM (50 mM KCl, 3 mM $MgCl_2$) to 147.5 mM with addition of Ficoll70. We measured the dependence of the reaction rate on the ionic strength, and fitted the experimental data with the Debye-Hückel equation, $k_{+6} = \exp(A\text{-}B\cdot[I]^{0.5})$, where I is the ionic strength, and A and B are fitting parameters (Figure S3). We found A = 1.16, B = 4.38 $M^{-0.5}$, and $k_{+6}^{I=147.5mM} = 0.6$ $\mu M^{-1}s^{-1}$. At I = 147.5 mM, the second order rate constant, k_{+6} is 2.8 times smaller than at the ionic strength of 59 mM. We conclude that the increased ionic strength alone does not explain the observed decrease in the rate of actin and myosin association in the crowded solution.

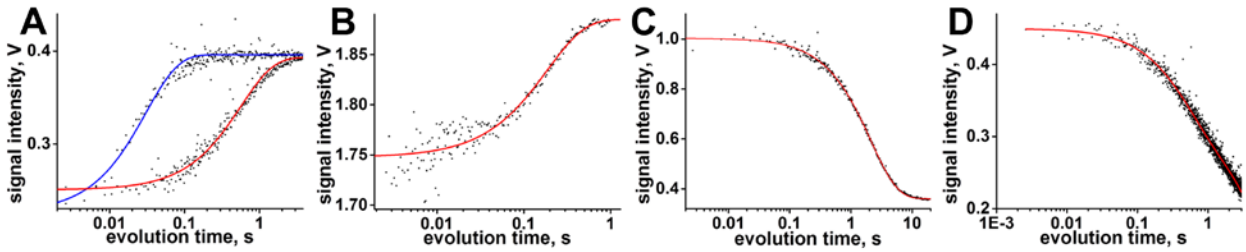

Figure S 1. (A) Transients of ATP-induced pyrene actomyosin dissociation, without (blue) and with (red) 37 μM ADP in solution. [actomyosin]=0.5 μM, [ATP]=25 μM. The lines represent single-exponential fits. The obtained rates are 32.8±1.0 s^{-1} and 1.77±0.04 s^{-1}, respectively.
(B) Intrinsic fluorescence transient after rapid mixing of 0.5 μM myosin and 18 μM ATP, step 3, Figure 2. Line, a single-exponential fit.
(C) Transient of the weak to strong binding transition of actomyosin (step 4, Figure 2) in a double mixing experiment. 3 μM myosin, prepared in the post-recovery M** state by rapid mixing with 100 μM ATP and following incubation of the reaction mixture for 2 s, rapidly mixed with 0.3 μM actin and 1 mM ADP to quench the reaction. Decrease of pyrene fluorescence shows kinetics of the strongly bound state formation. Line, a single-exponential fit.
(D) Transient of actomyosin rigor binding. 0.15 μM pyrene actin rapidly mixed with 0.9 μM myosin. Decrease of pyrene fluorescence shows the kinetics of the strongly bound state formation. Line, a single-exponential fit.

Electron paramagnetic resonance.

The frozen solution (T=15 K) field sweep spectrum of spin-labeled myosin (Figure S4) was acquired on the K_a-band pulsed EPR spectrometer at the University of Arizona [9], using a two-pulse electron spin echo technique. The experimental conditions were as follows: the mw pulses, 10 and 15 ns; time interval between the mw pulses, τ = 200 ns; boxcar integration gate, 15 ns. 30% w/v glycerol was added to the protein sample as a cryoprotectant. The low temperature powder spectrum was simulated to determine the principal values of the spin probe g- and hyperfine tensors [10], using a Monte-Carlo fitting routine implemented in Wolfram Mathematica 9 (Wolfram Research Inc, Champaign, IL). The room temperature (T≈20^{o}C) EPR spectra (Figure S5, Figure S6) were acquired with the X-band continuous wave EPR spectrometer Elexsys E500 (Bruker) at the EPR Facility of the University of Arizona. The experimental conditions were as follows: microwave frequency, 9.6 GHz; microwave power, 200 μW; modulation frequency, 100 kHz; modulation amplitude, 0.05 mT). Room temperature spectra of spin labeled F-actin and myosin with and without Ficoll70 were fitted using the magnetic tensors determined from the low-temperature spectrum fit using the NLSL software [11] in the model of microscopic order - macroscopic disorder (MOMD) [12], allowing the determination of the restrictions to the spin probe motion.

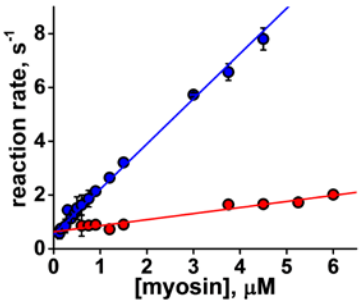

Figure S 2 The effect of Ficoll70 on actomyosin rigor binding kinetics. Linear fits. Blue, no Ficoll70, k_{+6}^{-F} = 1.68 ± 0.05 μM^{-1}s^{-1}, N=6. Red, with Ficoll70, k_{+6}^{+F} = 0.23 ± 0.03 μM^{-1}s^{-1}, N=3.

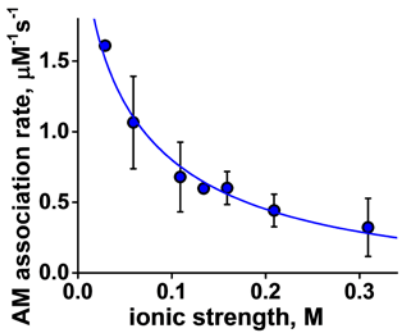

Figure S 3. Dependence of the rate of actomyosin rigor binding on the ionic strength of the solution. N=3. Fit to the equation k = exp(1.16 - 4.38 M$^{-0.5}$·[I]$^{0.5}$).

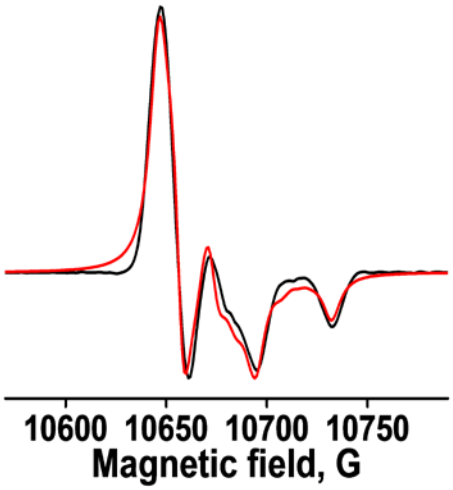

Figure S 4. K_a-band EPR spectrum of the maleimide TEMPO spin labeled myosin at T=15 K. Black, experiment, red, fit in the model of the powder spectrum to determine the magnetic tensors of the spin probe, g(2.00894, 2.00578, 2.00179), and A(6.07 G, 7.94 G, 37.52 G).

Actin structure is not affected by Ficoll70.

EPR of a nitroxide spin probe is a very sensitive method for characterizing structural changes in proteins [13, 14]. When a spin probe, bound to a protein, is located in the cleft between the protein subdomains, it is a good reporter on the subdomain reorganization. In actin, the labeling site C374 is located between subdomains 1 and 3, and an EPR study of spin-labeled actin can detect the possible structural effect of Ficoll70 on the relative orientation of the actin subdomains. Therefore, F-actin was labeled with TEMPO maleimide spin probe at C374 to

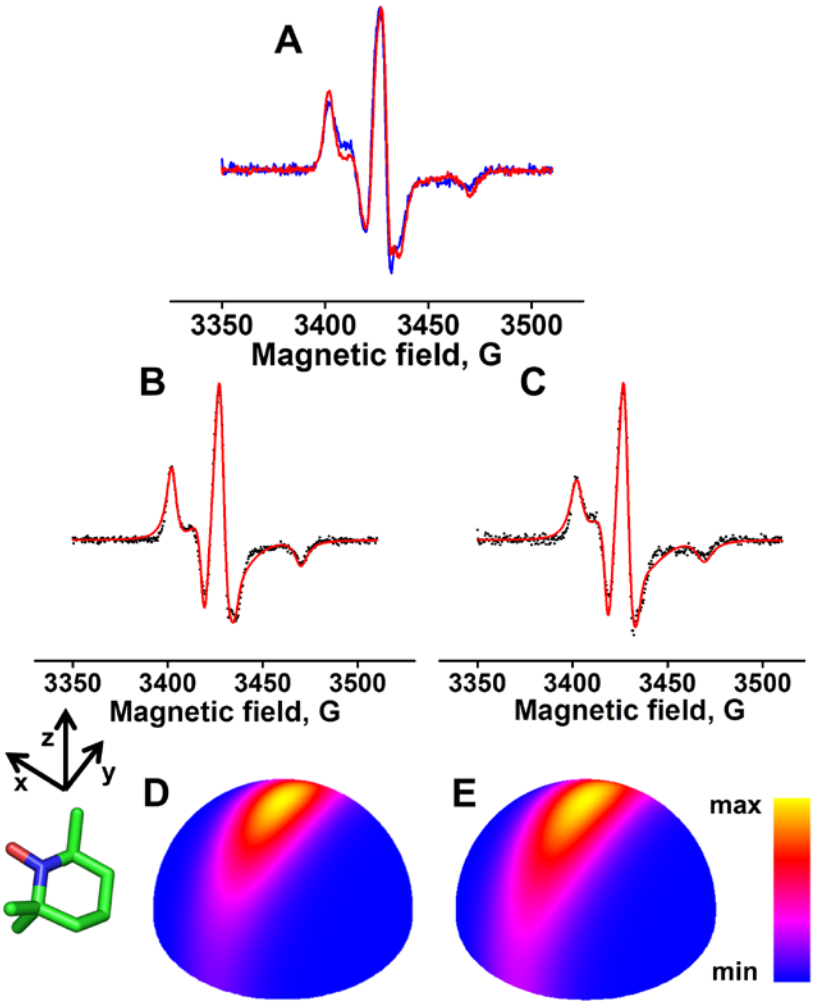

Figure S 5. A. X-band EPR spectra of the maleimide TEMPO spin probe at actin's C374, without (blue) and with (red) Ficoll70 in solution. C374 is located between actin's sub-domains 1 and 3, and the spin probe reflects Ficoll70-induced changes in actin structure. The magnitude of the outer extrema splitting is not affected by Ficoll70, indicating no change in the probe's mobility about its z axis. The minor changes in the inner splittings indicate slight differences in the probe's motion about x or y axes.
B,C, the fits of X-band spectra to determine the orientational distribution of the spin probe within actin's C374 labeling site, with (B) and without (C) Ficoll70 in solution. D and E, the orientational distributions of the spin probe with (D) and without (E) Ficoll70 in solution, based on the fits of the EPR spectra in the MOMD model. The probability of orientational distribution of z axis of the probe (perpendicular to the piperidine ring plane) is color-coded. With Ficoll70 in solution, the probe mobility about its x axis is slightly decreased.

determine if there are any changes in the probe's local structural environment when Ficoll70 is added to the solution. The X-band EPR spectra of spin-labeled F-actin with and without Ficoll70 are shown in Figure S5A. The simulations of X-band EPR spectra in the MOMD model (Figure S5, B and C) reveal highly anisotropic motion of the spin probe relative to actin molecular frame with the average correlation time of 33 ns. The order parameters [11] are D_{20} = 0.65 and D_{22} = -0.22 with Ficoll70, and D_{20} = 0.56 and D_{22} = -0.28 without Ficoll70; the probability of the orientational distribution of the spin probe within the actin monomer molecular frame is shown in Figure S5, D and E. Both spectral fits show the spin probe motion (rotational oscillations) mostly about its x-axis. There is a minor difference in the spin probe's restricted motion with and without Ficoll70: with Ficoll70 in solution, the oscillations about the x-axis have slightly smaller amplitude. In general, the spin probe has the same character of motion with and without Ficoll70, confirming that there is virtually no effect on the structure of F-actin in the presence of Ficoll70.

TR^{2}FRET data analysis.

In the TR^{2}FRET experiment, we observe the waveforms of the fluorescence of donor-acceptor labeled myosin in two structural states, M* and M**, and the fluorescence of donor-only labeled myosin. The acceptor (Dabcyl) is not fluorescent, and we do not expect to detect fluorescence from the acceptor. Therefore, the waveform of observed transient fluorescence at each time point is fitted as a sum of three components, convoluted with the instrument response function (determined from the light scatter).

The parameters of donor fluorescence are determined in a separate experiment with donor-only labeled myosin, using Eq. S1:

$$F_D(t) = \sum_{i=1}^{2} A_i \exp(-t/\tau_{Di}), \qquad \text{Eq. S1}$$

where τ_{Di} are the donor-only fluorescence lifetimes.

The interprobe distance and distance distribution $\rho(r)$ in the M* state are determined in the experiment with donor-acceptor labeled myosin without ATP, using Eq. S2. The donor fluorescence parameters determined in the previous experiment were kept fixed.

$$F_{DA}(t) = \int_0^{+\infty} \rho(r) \cdot \sum_{i=1}^{2} A_i \exp\left\{\left(-\frac{t}{\tau_{D_i}}\right) \cdot \left(1 + \left[\frac{R_0}{R}\right]^6\right)\right\} dr\,, \qquad \text{Eq. S2}$$

where R_0 = 4 nm is the Förster distance for IAEDANS-Dabcyl pair [15] and $\rho(r)$ is a probability density function to account for the interprobe distance distribution. We used a Gaussian distribution as a probability density function:

$$\rho(r) = \frac{1}{\sigma\sqrt{2\pi}} \exp\left(-\frac{(r-R)^2}{2\sigma^2}\right)\,, \qquad \text{Eq. S3}$$

where σ is the standard deviation, determining the interprobe distance distribution, and R is the position of the distribution maximum.

The mole fraction of the M** state, and the corresponding interprobe distance and distance distribution are determined from the experiment where myosin is rapidly mixed with ATP. Experimental data are fitted by Eq. S4, with all previously determined parameters fixed.

$$F_{total}(t) = X \cdot F_D(t) + X^* \cdot F_{DA^*}(t) + X^{**} \cdot F_{DA^{**}}(t), \quad X + X^* + X^{**} = 1, \qquad \text{Eq. S4}$$

In this equation, X without and with superscripts are the mole fractions of donor-donor labeled myosin (X), and donor-acceptor labeled myosin in M* and M** structural states.

To account for Ficoll70 photobleaching, we collected the waveforms of Ficoll70 fluorescence at the same wavelength and intensity of the excitation light, and the same spectral range and voltage of the detector as in the experiments with myosin. The obtained waveforms of Ficoll70 fluorescence were fitted with single-exponential functions with a constant decay time constant convoluted with the instrument response function. Intensities of Ficoll70 fluorescence waveforms were fitted by a polynomial (Figure S9), and this completely characterized Ficoll70 fluorescence signal was accounted for in the global fit of the FRET effect of the donor-acceptor pair within myosin head.

Analysis of transient time-resolved fluorescence data was performed using software package FargoFit, designed by I. Negrashov, that executes global least-square fitting of multiple time-resolved fluorescence waveforms using different kinetic models with ability to link fitting parameters between waveforms.

Förster distance calculation.

The Förster distance, R_0, was calculated as

$$R_0 = 9786[J(\lambda)\kappa^2\eta^{-4}Q_D]^{1/6}, \qquad \text{Eq. S5}$$

where λ is the wavelength, $J(\lambda)$ is the spectral overlap integral between normalized donor emission spectrum $F_D(\lambda)$ and the acceptor absorption spectrum $\varepsilon_A(\lambda)$ [15], $\kappa^2 = 2/3$ is the probes orientation factor, $\eta = 1.4$ is the refraction index of the medium, Q_D is the donor quantum yield [15]. To ensure that the R_0 does not change upon Ficoll70 addition to the solvent we checked the spectra of donor emission and acceptor absorption, and compared the level of donor fluorescence in the presence and absence of Ficoll70. Fluorescence of Ficoll70 was subtracted from the donor fluorescence. Donor and acceptor spectra were the same with and without Ficoll70 [15], therefore the spectral overlap integral is not affected by Ficoll70 addition. The magnitude of the donor fluorescence was the same with and without Ficoll70, therefore the donor quantum yield was not disturbed by addition of Ficoll70. The index of refraction of the solution changes marginally (3%) with addition of 25% w/v Ficoll70 [16], this change of the index virtually does not affect R_0. The κ^2 factor determines averaged relative orientation of the donor and acceptor and the average value of $\kappa^2 = 2/3$ corresponds to the model of donor and acceptor probes independently sampling all possible orientations. We used EPR to examine if addition of Ficoll70 affects the probability of orientational distribution of a probe at the myosin labeling site. Single Cys myosin mutant K498C was labeled with the maleimide TEMPO spin probe and X-band EPR spectra were acquired for spin labeled myosin in buffered solution with and without 25% w/v Ficoll70 (Figure S6). The spectra show virtually no change in the probe mobility with addition of Ficoll70 to the solution, indicating no major effect of Ficoll70 on the factor κ^2. Therefore we conclude that R_0 does not change with addition of Ficoll70 to the buffer.

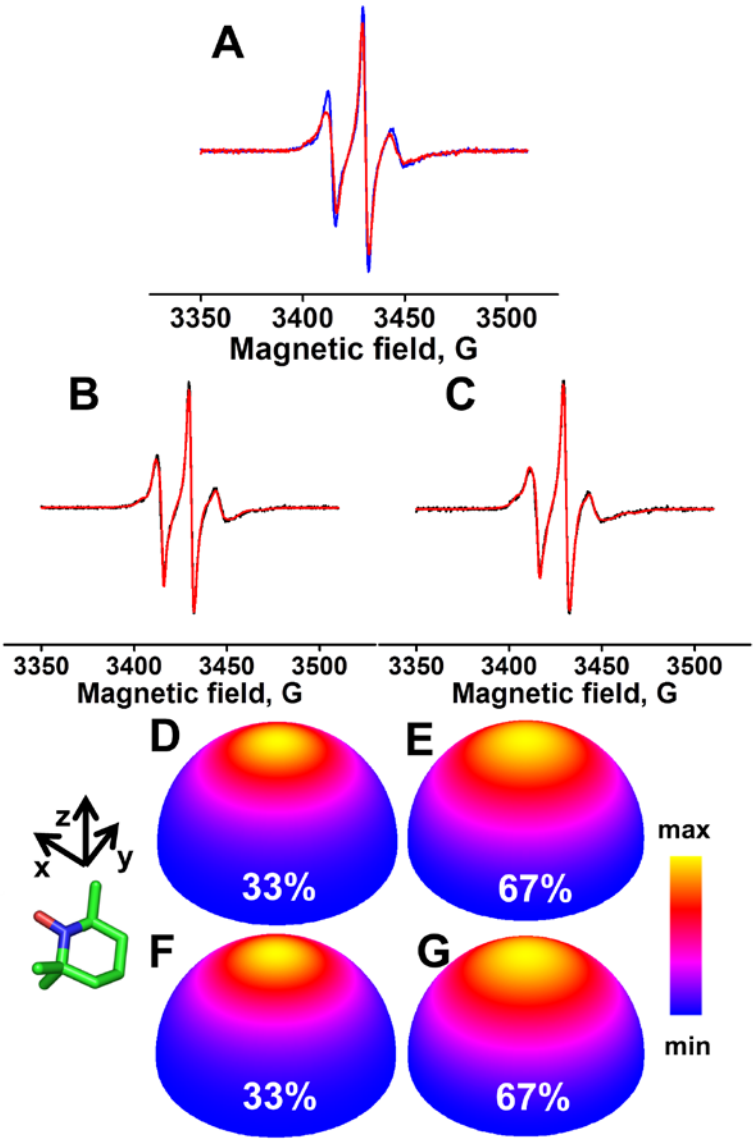

Figure S 6. A. X-band EPR spectra of myosin labeled at K498C with maleimide TEMPO spin probe, without (blue) and with (red) Ficoll70 in solution. Both spectra show two conformations of the spin probe with the distinct slow (restricted) and fast (less restricted) motion. B, C. The fit of both spectra using MOMD model, B, without Ficoll70; C, with Ficoll70. D-G. Spin probe orientational distribution in the myosin molecular frame obtained from the fits. The fits show that the spectral components corresponding to the slow and restricted motion of the spin probe (33% of total spin probe population, D, without Ficoll70, and F, with Ficoll70) are not affected by Ficoll70. The correlation time of the spin probe motion is 27.5 ns and the isotropic order parameter is D_{20} = 0.53. The order parameter of the spectral components, corresponding to the fast (correlation time 7.9 ns) and less restricted motion (E, without Ficoll70, and G, with Ficoll70) depends on the presence of Ficoll70 in solution, the isotropic order parameter D_{20} changes from D_{20} = 0.19 without Ficoll70 (E), to D_{20} = 0.22 with Ficoll70 (G). X-band EPR spectra reflect global tumbling of myosin molecule [14] and such small increase of the order parameter with addition of Ficoll70 may reflect the viscosity change. The orientational distribution of z axis of the probe (perpendicular to the piperidine ring plane) is color-coded.

Steady state ATPase assays.

Concentration of ATP in both basal and actin activated myosin ATPase was 5 mM, myosin concentration was 3.3 μM in the basal and 0.84 μM in the actin activated myosin ATPase. From 4.2 μM to 84 μM actin (5x – 100x) was used in the actin activated ATPase. At the time point zero myosin or actomyosin was mixed with ATP, and aliquots were collected at equal time intervals. The solution was incubated at T = 20°C. After collection, the aliquots were immediately mixed with the malachite green – ammonium molybdate solution (0.06% malachite green carbinol hydrochloride, 15 mM ammonium molybdate tetrahydrate in 1N HCl, with 4% of 1% Sterox detergent, added immediately before use), the mixture was quenched with 34% sodium citrate in 1N HCl after 30 seconds of color development. Then the aliquots were incubated 20 minutes at room temperature before measurement of optical density at 620 nm. To interpret results of optical density measurement at 620 nm in terms of phosphate concentration, a calibration curve was measured using the same colorimetric assay with premixed phosphate solutions of known concentration. The typical time dependence of actin activated myosin ATPase is shown in Figure S7. Obtained data of optical density were fitted with the straight lines, to determine the rate of color development in the course of ATPase, then the rates were recalculated in terms of concentration of the phosphate produced in the reaction, using the calibration curve. Normalization on the amount of myosin in the assay gives the rate of the phosphate production per myosin head. Straight lines in Figure S7 confirm that the presence of ADP, produced in the reaction, does not perturb the reaction. 5 mM ATP is clearly a saturating concentration, and the velocity of the reaction is not affected by ADP contamination [17].

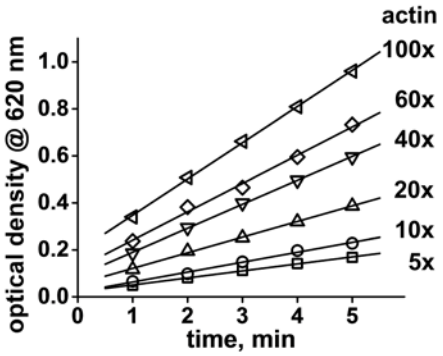

Figure S 7. Typical time dependence of the actin activated myosin ATPase at different actin concentrations. [Myosin] = 0.84 μM, [ATP] = 5 mM. The sensitivity of the assay is 3.5 μM phosphate in solution. Linear fits confirm that 5 mM ATP is truly saturating concentration and the production of ADP in the course of the reaction does not affect the V_{max}.

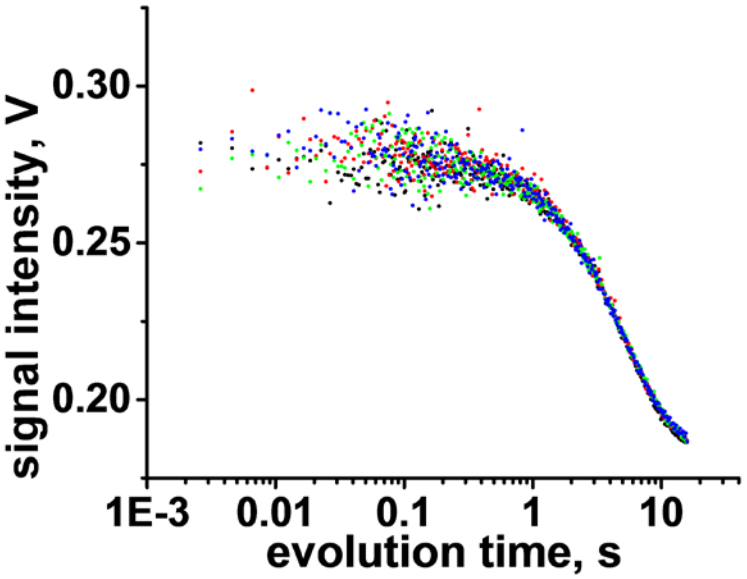

Figure S 8. Calibration of the delay time in the weak to strong actomyosin binding transition experiment. The decrease of pyrene actin fluorescence reflects the strong actomyosin binding. Double mixing experiment: in the first rapid mixing of myosin and ATP, myosin is prepared in the post-recovery stroke state M**. The mixture is aged to maximize [M**]. Then the initial mixture is rapidly mixed with pyrene actin and ADP. ADP is added to stop actomyosin ATPase activity after formation of the strongly bound state. Overlay of weak to strong binding transients at different delay times: black, 0.7 s; red, 2 s; green, 5 s; blue, 10 s. All transients are similar and show no dependence on the delay time.

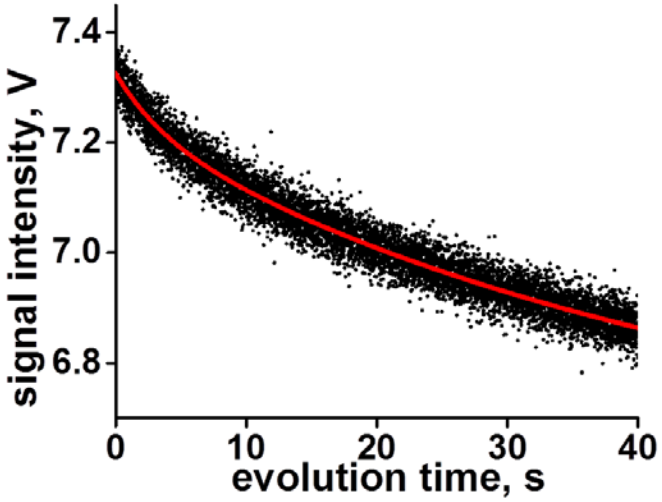

Figure S 9. Photobleaching of the 25% w/v Ficoll70 buffered solution. Excitation wavelength 365 nm, the signal is detected using a 420 nm cutoff filter. Red line is a polynomial fit. Ficoll70 photobleaching transient was acquired for each buffer preparation, and the fitted line was subtracted from the raw transients of pyrene labeled actin in actomyosin binding and dissociation experiments. Ficoll70 concentration, flow rate, intensity and the wavelength of the excitation light, the detector voltage and the spectral range of the detected light were kept the same in all experiments.

Supporting References

1. Criddle, A.H., M.A. Geeves, and T. Jeffries, *The Use of Actin Labeled with N-(1-Pyrenyl)Iodoacetamide to Study the Interaction of Actin with Myosin Subfragments and Troponin Tropomyosin.* Biochemical Journal, 1985. **232**(2): p. 343-349.
2. Deacon, J.C., et al., *Erratum to: Identification of functional differences between recombinant human alpha and beta cardiac myosin motors.* Cell Mol Life Sci, 2012. **69**(24): p. 4239-55.
3. Woodward, S.K.A., M.A. Geeves, and D.J. Manstein, *Kinetic characterization of the catalytic domain of Dictyostelium discoideum myosin.* Biochemistry, 1995. **34**(49): p. 16056-16064.
4. Gyimesi, M., et al., *Kinetic characterization of the function of myosin loop 4 in the actin-myosin interaction.* Biochemistry, 2008. **47**(1): p. 283-91.
5. Kurzawa, S.E., D.J. Manstein, and M.A. Geeves, *Dictyostelium discoideum myosin II: characterization of functional myosin motor fragments.* Biochemistry, 1997. **36**(2): p. 317-23.
6. Liu, X., et al., *Biological, biochemical, and kinetic effects of mutations of the cardiomyopathy loop of Dictyostelium myosin II: importance of ALA400.* J Biol Chem, 2005. **280**(29): p. 26974-83.
7. Siemankowski, R.F. and H.D. White, *Kinetics of the interaction between actin, ADP, and cardiac myosin-S1.* J Biol Chem, 1984. **259**(8): p. 5045-53.
8. Wenner, J.R. and V.A. Bloomfield, *Crowding effects on EcoRV kinetics and binding.* Biophys J, 1999. **77**(6): p. 3234-41.
9. Astashkin, A.V., J.H. Enemark, and A.M. Raitsimring, *26.5–40 GHz Ka-band pulsed EPR spectrometer.* Concepts in Magnetic Resonance Part B: Magnetic Resonance Engineering, 2006. **29B**: p. 125-136.
10. Libertini, L. and O. Griffith, *Orientation dependence of the electron spin resonance spectrum of di-t-butyl nitroxide.* J Chem Phys, 1970. **53**: p. 1359-1367.
11. Budil, D., et al., *Nonlinear-least-squares analysis of slow-motion EPR spectra in one and two dimensions using a modified Levenberg-Marquardt algorithm.* J Magn Reson, 1996. **A120**: p. 155-189.
12. Schneider, D.J. and J.H. Freed, *Calculating slow motional magnetic resonance spectra: a user's guide*, in *Biological Magnetic Resonance*, L.J. Berliner, Editor. 1989, Plenum Publishing Corporation. p. 1-76.
13. Nesmelov, Y.E., *Protein structural dynamics revealed by site-directed spin labeling and multifrequency EPR.* Methods Mol Biol, 2014. **1084**: p. 63-79.
14. Nesmelov, Y.E., et al., *Structure and dynamics of the force-generating domain of myosin probed by multifrequency electron paramagnetic resonance.* Biophys J, 2008. **95**(1): p. 247-56.
15. Agafonov, R.V., et al., *Structural dynamics of the myosin relay helix by time-resolved EPR and FRET.* Proc Natl Acad Sci U S A, 2009. **106**(51): p. 21625-30.
16. Georgalis, Y., et al., *Light scattering studies on Ficoll PM70 solutions reveal two distinct diffusive modes.* Journal of Colloid and Interface Science, 2012. **386**: p. 141-147.
17. Segel, I.H., *Biochemical Calculations*. 1976: Wiley.